Bioactive Materials 20 (2023) 598–609

Contents lists available at ScienceDirect

Bioactive Materials

journal homepage: www.keaipublishing.com/en/journals/bioactive-materials

Carboxymethyl chitosan-alginate enhances bone repair effects of magnesium phosphate bone cement by activating the FAK-Wnt pathway

Ling Yu [a,d,1], Tian Gao [b,1], Wei Li [a,1], Jian Yang [a], Yinchu Liu [a], Yanan Zhao [c], Ping He [d], Xuefeng Li [d], Weichun Guo [a,**], Zhengfu Fan [b,*], Honglian Dai [c,***]

[a] Department of Orthopedic Surgery I (Spine Surgery), Renmin Hospital of Wuhan University, Wuhan, 430060, China
[b] Department of Orthopedic Oncology, Key Laboratory of Carcinogenesis and Translational Research, Ministry of Education, Peking University Cancer Hospital & Institute, Beijing, 100000, China
[c] State Key Laboratory of Advanced Technology for Materials Synthesis and Processing, Biomedical Materials and Engineering Research Center of Hubei Province, Wuhan University of Technology, Wuhan, 430070, China
[d] Department of Orthopedic Surgery, Renmin Hospital of Shayang, Jingmen, 448200, China

ARTICLE INFO

Keywords:
Critical bone defect
Magnesium phosphate cement
Carboxymethyl chitosan
Sodium alginate
Osteogenic differentiation

ABSTRACT

There is a continuing need for artificial bone substitutes for bone repair and reconstruction, Magnesium phosphate bone cement (MPC) has exceptional degradable properties and exhibits promising biocompatibility. However, its mechanical strength needs improved and its low osteo-inductive potential limits its therapeutic application in bone regeneration. We functionally modified MPC by using a polymeric carboxymethyl chitosan-sodium alginate (CMCS/SA) gel network. This had the advantages of: improved compressive strength, ease of handling, and an optimized interface for bioactive bone in-growth. The new composites with 2% CMCS/SA showed the most favorable physicochemical properties, including mechanical strength, wash-out resistance, setting time, injectable time and heat release. Biologically, the composite promoted the attachment and proliferation of osteoblast cells. It was also found to induce osteogenic differentiation *in vitro*, as verified by expression of osteogenic markers. In terms of molecular mechanisms, data showed that new bone cement activated the Wnt pathway through inhibition of the phosphorylation of β-catenin, which is dependent on focal adhesion kinase. Through micro-computed tomography and histological analysis, we found that the MPC-CMCS/SA scaffolds, compared with MPC alone, showed increased bone regeneration in a rat calvarial defect model. Overall, our study suggested that the novel composite had potential to help repair critical bone defects in clinical practice.

1. Introduction

Bone defects are caused by multiple diseases, such as trauma, tumors and infection. It is believed that self-repair is impossible when bone defects exceed a critical size, and require further clinical intervention [1,2]. Traditionally, autologous and allogeneic bone transplantation is the main choice of treatment for these defects; however, it has many disadvantages, such as limited sources, bone removal-related complications, potential disease transmission risk, and immune rejection [3,4]. Nowadays, there is a tendency towards the application of artificial bone-graft substitutes in critical bone defects [5,6].

Calcium phosphate cements (CPC) have been widely used for bone repair owing to their similarity to hydroxyapatite (HA) in natural bone [7,8]. However, their weak strength, long clotting time and slow adsorption hinder their further clinical application [9,10]. Therefore, it is important to explore and discover new orthopedic implants with higher biological activity, faster degradation rate, and suitable mechanical properties.

Magnesium is an essential element that plays a vital role in bone health and ~60% of magnesium is stored in the bone matrix [11,12].

Peer review under responsibility of KeAi Communications Co., Ltd.
* Corresponding author.
** Corresponding author.
*** Corresponding author.
E-mail addresses: guoweichun@aliyun.com (W. Guo), zhengfufan@126.com (Z. Fan), daihonglian@whut.edu (H. Dai).
[1] These authors contributed equally to this work.

https://doi.org/10.1016/j.bioactmat.2022.06.017
Received 25 May 2022; Received in revised form 22 June 2022; Accepted 23 June 2022

Researchers have developed magnesium-based alloys to enhance osteogenic effects [13]. For instance, Zhang et al. found that magnesium promoted bone fracture healing through upregulation of neuronal calcitonin gene-related polypeptide [14]. Qiao et al. reported that magnesium led to the formation of a pro-osteogenic immune microenvironment in a transient receptor potential cation channel member 7 (TRPM7)-dependent manner [15]. Researchers have been attracted by magnesium phosphate cement (MPC), which has high mechanical strength and degradability [16]. Many studies have evaluated MPC as an inorganic bone filler *in vitro* and *in vivo*, and confirmed its favorable biocompatibility and biodegradability [17–19]. However, the fast setting and rapid heat release of MPC make its clinical application unfavorable. In particular, the mechanical strength and osteo-inductivity for bone regeneration need improvement.

Natural bone tissue consists of proteins and inorganic minerals. Biomaterials aim to replicate the physical structure and/or functions of the protein and mineral in order to promote and support the growth of new bone and restore its function [20]. For example, the addition of hyaluronic acid to CPC improves its compressive strength and increases osteogenesis through upregulation of osteogenic gene expression [9]. Therefore, MPC can be combined with other organic biomaterials to imitate bone structure so as to improve its bone regenerative capacity. Among those natural polymers, carboxymethyl chitosan (CMCS) and sodium alginate (SA) are of particular interest in medicine and biotechnology. Due to their biocompatibility, low toxicity and easy obtainability, both of them have been extensively investigated in wound healing, drug delivery and tissue engineering [21–23]. CMCS is a carboxymethyl-modified water-soluble derivative of chitosan with positively charged amino groups, its structure resembles glycosaminoglycans in extracellular matrix (ECM), which supports cell adhesion and

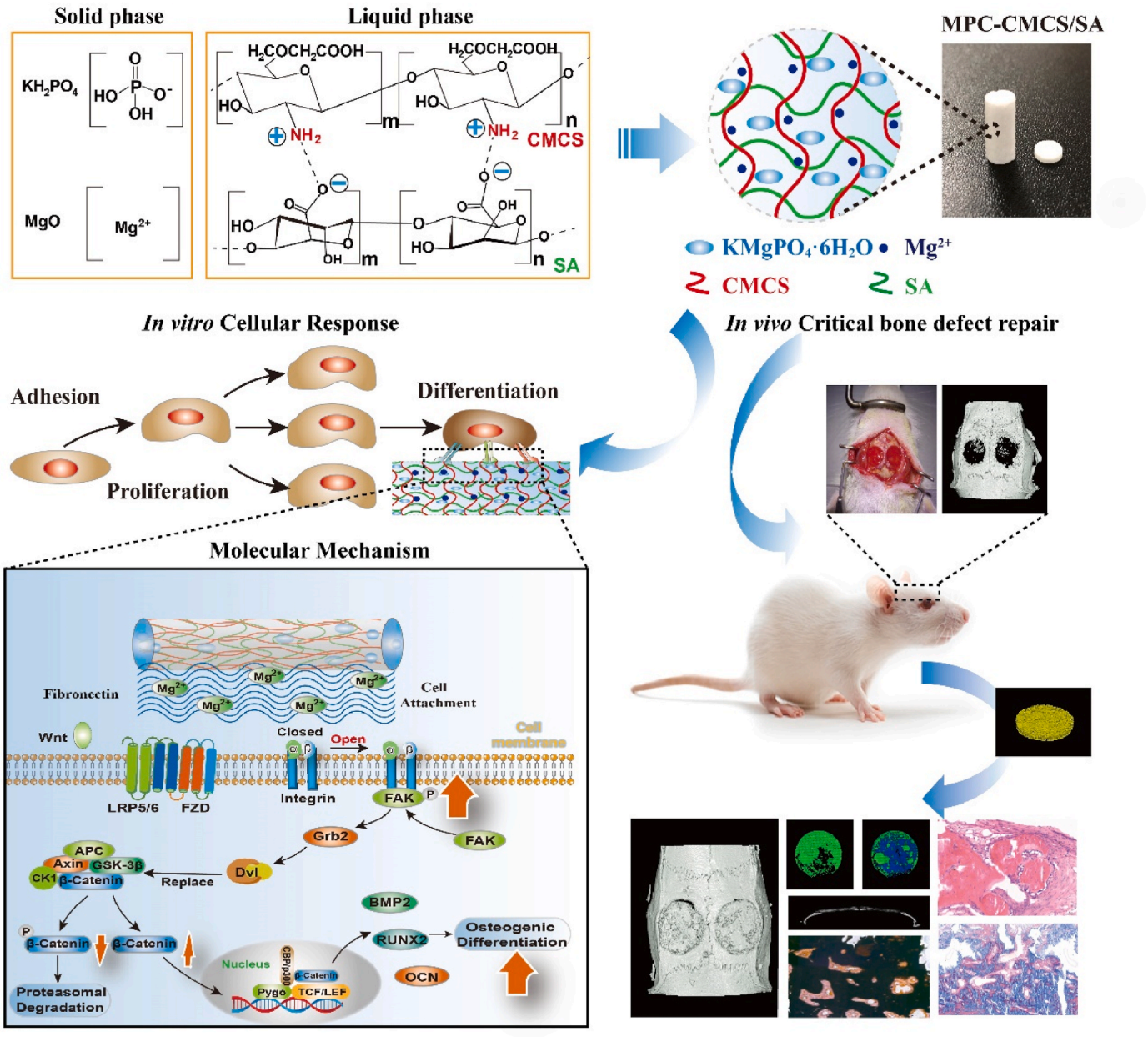

Scheme 1. Schematic illustration of the study. The MPC solid phase consisted of KH_2PO_4 and dead burned MgO. The liquid phase was obtained by dissolving CMCS and SA in distilled water. The solid and liquid phases were thoroughly mixed, stirred and self-set. The biocompatibility and ability to modulate cell adhesion, proliferation and differentiation of the resulting MPC-CMCS/SA composites were examined. In addition, we found that the composites promoted osteogenic differentiation via the FAK-Wnt axis. Eventually, using a rat calvaria defect model, the *in vivo* bone repair capability was estimated.

proliferation [24,25]. SA is composed of different ratios of (1–4')-linked β-D-mannuronate (M) and α-L-guluronic acid ester (G) moieties and shows negatively charged carboxyl groups. The G-blocks in SA have crosslinking affinity, which could form hydrogels with divalent cations such as Ca^{2+} and Mg^{2+} [26]. Combination of CMCS and SA forms strong electrostatic interactions due to their oppositely charged groups [27–29].

Previously, we optimized MPC with CMCS, and found that CMCS improved both the physicochemical properties and biocompatibility. Unfortunately, CMCS-MPC composites are inefficient in their bonding at interfaces, and the compressive strength of the composites and their biological performance need improvement [30].

Previously, chitosan-alginate complexes have been used to enhance the properties of inorganic biomaterials, such as hydroxyapatite [31–33]. Nevertheless, to our knowledge, this is the first attempt to combine CMCS/SA hydrogels with magnesium-based cement systems. This study tested the resulting MPC-CMCS/SA composites for their biocompatibility and ability to modulate cell adhesion, proliferation and differentiation. In addition, the molecular mechanisms that promoted osteogenic differentiation were investigated. Finally, *in vivo* osteogenic efficacy was estimated using a rat calvarial defect model (Scheme 1).

2. Materials and methods

2.1. MPC preparation

The MPC solid phase consisted of dead burned magnesia (MgO; purity 98.5%, calcinated at 1600 °C for 4 h) and potassium dihydrogen phosphate (KH_2PO_4; purity 99.5%) with a molar ratio of 1.5:1(Sinopharm Chemical Reagents, Shanghai, China). The composite material was put into a ball mill for grinding and sieved with 200 mesh to obtain particles of ~75 μm. The polymer complex resulting from the reaction between CMCS and SA (Sinopharm Chemical Reagents, Shanghai, China) was used as the aqueous source for the MPC reaction (Table 1). The solid and liquid phases were thoroughly mixed with a powder/liquid ratio (P/L) of 2 (g/ml), stirred into a uniform paste, and transferred to cylindrical molds. Finally, all samples were set at 37 °C, 100% relative humidity for 72 h before subsequent experiments.

2.2. Chemical composition and surface morphology

The hardened bone cement was ground into powder and X-ray diffraction analysis (XRD; XPert Pro, Almelo, Netherlands) was performed to assess the MPC-CMCS/SA composition over a 2θ range of 10–65° using Cu–K α radiation with a voltage of 40 kV and a current of 50 mA. Chemical composition analysis was performed using Fourier transform infrared spectroscopy (FT-IR; Thermo Fisher Scientific, MA, USA). The samples and KBr powder were pressed into a tablet, and the infrared spectrum of the tablet was tested in the range of 4000 to 500 cm^{-1}. The surface morphology of cement samples was observed by scanning electron microscopy (SEM; Carl Zeiss, Cambridge, UK).

2.3. Setting time and thermal measurements

The solidification time was defined as the time taken before a needle could not penetrate 1 mm into the sample using a Vicat instrument according to the Chinese National Standard (GB/T1346-2001). The hydration temperature was measured at 37 °C with a thermocouple (WZPZ-236, SICK, Waldkirch, Germany) placed in the middle of the cement paste at 37 °C, and the paste was placed in a polystyrene mold for temperature insulation. Values were obtained from at least three independent samples.

Table 1
Compositions of setting liquids for cements.

Samples	CMCS (wt%)	SA (wt%)
MPC	0	0
MPC-CMCS/SA (1%)	1	1
MPC-CMCS/SA (2%)	2	2
MPC-CMCS/SA (3%)	3	3
MPC-CMCS/SA (4%)	4	4

2.4. Mg^{2+} release and pH variation

For Mg^{2+} release and pH analysis, 100 μl of solution was removed at the indicated time points and the ion concentration of magnesium (Mg^{2+}) measured with an atomic absorption spectrophotometer (ContrAA700; Analytik Jena, Jena, Germany) and the pH value of the medium measured using a pH meter (PHS-25; INESA, Shanghai, China).

2.5. Injectability and wash-out resistance

The injectability was assessed by manually pushing the paste-like MPC-CMCS/SA through 5-mL syringe. The injectable time was assessed as the duration from the formation of the paste which could be injected continuously until the paste completely solidified and could not be injected. The washout resistance was tested by injecting the paste into Ringer's solution, and the integration of the composites was observed for 30 min.

2.6. Compressive strength and cement degradation in vitro

The compressive strength of the sample was measured at a loading rate of 1 mm/min using a universal testing machine (SHT4 605, MTS Systems, MN, USA) according to standards proposed by the British Standards Authority. To assess the *in vitro* degradation of various scaffolds, the samples were immersed in saline solution and dried at the indicated time points (days 1, 3, 5, 7, 14, 21 and 28). The degradation rate was calculated as the percentage of the weight loss to initial weight. Testing values were calculated from at least three independent samples.

2.7. In vitro studies

2.7.1. Cell proliferation

MC3T3-E1 pre-osteoblast cells (ATCC; CRL-2595) were cultured in α-minimal essential medium M (Hyclone; GE Healthcare, IL, USA) containing 10% fetal bovine serum (FBS; Gibco, MA, USA), 100 U/mL penicillin, and 100 μg/mL streptomycin. Cells were grown in a humidified atmosphere containing 5% CO_2 at 37 °C. All samples were sterilized prior to cell seeding. Cells were then seeded at 10^4/well, and incubated for 1, 3 and 5 days. 10 μl Cell Counting Kit-8 (CCK-8; Dojindo Laboratories, Kumamoto, Japan) was incubated with the cells for 2 h at 37 °C. The optical density was measured at 450 nm using a microplate reader.

2.7.2. Cell morphology

Samples were washed and fixed in 4% paraformaldehyde, dehydrated with graded alcohol, and oven dried. Samples were observed by scanning electron microscopy (SEM; Carl Zeiss, Cambridge, UK) after vacuum spraying with gold.

2.7.3. Immunofluorescence microscopy

Cells were fixed with 4% paraformaldehyde for 15 min and washed three times with PBS. F-actin was stained with acti-stain 555 phalloidin (Servicebio, Wuhan, China) for 1 h, while nuclei were counterstained by 4′,6-diamidino-2-phenylindole (DAPI). Afterwards, the fluorescence images were observed and captured using fluorescence microscopy (FV1200; Olympus, Tokyo, Japan).

2.7.4. Quantitative real-time polymerase chain reaction

Total RNA was extracted using TRIzol (Invitrogen; 15596026) reagent, and cDNA was synthesized with the RevertAid™ first strand

cDNA synthesis kit (Thermo Scientific; K1622). Real-time polymerase chain reaction (PCR) was performed using the ABI PRISM 7900HT sequence detection system (Applied Biosystems, CA, USA). The expression of osteogenesis-related genes was normalized to GAPDH using the $2^{-\Delta\Delta CT}$ method. The primer sequences are listed in Table 2.

2.7.5. Western blotting

Protein (40 μg) was extracted using protein lysis buffer (Beyotime, Beijing, China), separated by 10% SDS-PAGE and transferred to polyvinylidene difluoride (PVDF) membranes. The membranes were blocked with 5% skimmed milk, followed by incubation with primary antibodies at 4 °C overnight. The membranes were incubated with horseradish peroxidase-conjugated secondary antibodies for 2 h. Blots were developed using the ECL system (Amersham Biosciences, Little Chalfont, UK). The antibodies used in our study were purchased from Abcam (Cambridge, UK), including anti-β-catenin (phospho Y489) antibody (ab119801), anti-β-catenin antibody ab265591), anti-focal adhesion kinase (FAK) (phospho Y397) antibody (ab81298), anti-FAK antibody (ab40794), anti-bone morphogenetic protein (BMP2) antibody (ab214821), anti-osteocalcin (OCN) antibody (ab133612), anti-Runt-related transcription factor (RUNX2) antibody (ab264077). GAPDH was selected as internal reference gene. All experiments were repeated at least three times.

2.8. In vivo experiments

2.8.1. Experimental procedures

All *in vivo* experiments were reviewed and approved by the Investigational Ethical Review Board of Renmin Hospital of Wuhan University. Twenty-four Sprague-Dawley rats were randomized into two groups (n = 12 per group): MPC and MPC-CMCS/SA (2%). Rats were anesthetized by intraperitoneal injection of 100 mg/kg ketamine and 10 mg/kg xylazine. After successful anesthesia, a 3-cm midline incision was made through the sagittal suture, and the bilateral calvaria bones were exposed. Full-thickness bone defects were bilaterally created using a 6.0 mm-diameter dental drill. MPC and MPC-CMCS/SA (2%) cements (1 mm thickness) were placed into the defects **(Suppl Fig. 1A–B)**. Finally, the incisions were closed. After 1 and 3 months of implantation, the calvaria bones were dissected for further analysis.

2.8.2. Micro-computed tomography

The dissected calvaria were subject to micro-computed tomography (ScanXmate-E090S40; Comscantecno, Kanagawa, Japan). Image data were transferred for 3D reconstruction and image analysis. Bone volume/total volume (BV/TV) and structural bone parameters, including trabecular thickness (Tb.Th), trabecular number (Tb.N), and trabecular separation (Tb.Sp), were calculated.

2.8.3. Histological analysis

The dissected calvaria were fixed and embedded in paraffin without decalcification. A hard tissue microtome (Leica SP1600; Leica Biosystems, Nussloch, Germany) was used to obtain paraffin sections of 10 μm. After deparaffinization, they were rinsed five times before staining with Hematoxylin and Eosin (H&E), von Kossa and Masson. Images of sections were observed under a microscope and captured using a digital camera (Olympus BX51; Olympus, Tokyo, Japan).

Table 2
Primer sequences used in quantitative PCR assay.

Gene	Sequence(5′-3′)
BMP2	Forward primer:CCACCATGAAGAATCTTTGGA
	Reverse primer:GTGATAAACTCCTCCGTGG
OCN	Forward primer:GGTGCAGACCTAGCAGACACCA
	Reverse primer:AGGTAGCGCCGGAGTCTATTCA
RUNX2	Forward primer:CCATAACGGTCTTCACAAATCCT
	Reverse primer:TCTGTCTGTGCCTTCTTGGTTC
GAPDH	Forward primer:GGCACAGTCAAGGCTGAGAATG
	Reverse primer:ATGGTGGTGAAGACGCCAGTA

2.9. Statistical analysis

The data were shown as means ± SD. The difference was analyzed using the Student's t-test, one-way or two-way analysis of variance (ANOVA), and $p < 0.05$ was considered statistically significant.

3. Results

3.1. Physicochemical characterization of MPC-CMCS/SA scaffolds

3.1.1. Mechanical properties and self-setting behavior of the scaffolds

We showed that adding polymer complex to the cement system enhanced its handling properties in various ways. The compressive strength of the cements is shown in Fig. 1A. With the increase of CMCS and SA, the compressive strength increased initially and then decreased. MPC-CMCS/SA (2%) achieved the highest compressive strength of 59.43 ± 8.31 MPa on the day 5, whereas MPC-CMCS/SA (4%) decreased to an average of <50 MPa. The wash-out resistance of the MPC initially increased and then decreased, with 2% CMCS/SA incorporation showed the best performance (Fig. 1B).

Within the concentration range of 1–4%, addition of CMCS/SA had no effect on *in vitro* degradation, release of Mg^{2+} and pH value (Fig. 2A-C). The setting time of MPC was 3.40 ± 0.66 min, which was significantly increased by addition of CMCS/SA. The setting time of MPC-CMCS/SA (4%) reached 12.83 ± 1.63 min (Fig. 2D). The injectable time of MPC-CMCS/SA composite was prolonged significantly by the increase in CMCS/SA, and increased from 0.50 ± 0.10 min (MPC alone) to 2.87 ± 0.21 min with 4% CMCS/SA (Fig. 2E). The maximum temperature of MPC reached 64.00 ± 6.71 °C. However, as the setting process extended, adding CMCS and SA reduced the maximum temperature, with MPC-CMCS/SA (4%) decreased to 39.43 ± 8.30 °C (Fig. 2F).

3.1.2. Structure and morphology of the scaffolds

As shown in Fig. 3A, the characteristic peaks of $KMgPO_4{\cdot}6H_2O$ and unreacted MgO were both observed in the MPC and MPC-CMCS/SA scaffolds. However, due to the low content of these two components, the characteristic absorption bands of CMCS and SA were not observed in the XDR spectra of the corresponding composites. The FT-IR spectra of MPC, MPC-CMCS, MPC-SA, and MPC-CMCS/SA are shown in Fig. 3B. The spectrum of MPC products showed the characteristic peaks of PO_4^{3-} stretching ranging from 993 to 1012 cm^{-1}, and the stretching vibrations of Mg–O at 572 cm^{-1}. The wide-ranging bands of 3700-2500 cm^{-1} and 1800 to 1500 cm^{-1} indicated the H_2O molecules (H–O–H). There were two characteristic peaks of the SA at 1595 cm^{-1} and 1408 cm^{-1}, corresponding to the -COO^- asymmetric and symmetric stretching. The spectrum of MPC-SA and MPC-CMCS/SA showed a normal symmetric stretching peak but a shift of COO^- asymmetric stretching peak to a higher wave number (from 1595 to 1633 cm^{-1}). The spectrum of MPC-CMCS showed the characteristic peaks of CMCS at 1627 cm^{-1} and at 1101 cm^{-1}, corresponding to the NH_2 variable angle vibrating and the C–O–C symmetric stretching. The spectrum of MPC-CMCS/SA showed a shift of the variable angle vibration of NH_2 to the asymmetric variable angle vibration of NH_3^+ at 1680 cm^{-1}.

The morphology of the different composites was observed using SEM. MPC was mainly composed of Struvite-(K) crystals with numerous cracks (Fig. 4). Addition of CMCS/SA filled the cracks and made the surface of the composites smoother.

3.2. In vitro evaluation of MPC-CMCS/SA scaffolds

3.2.1. Cell adhesion and proliferation on samples

Cell morphology and adhesion were assessed using fluorescence

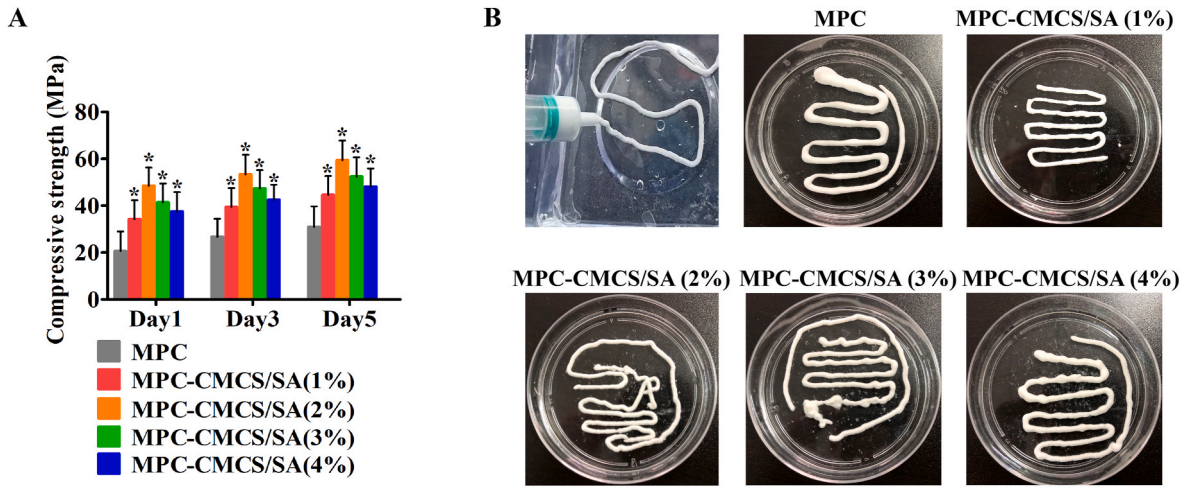

Fig. 1. (A) Compressive strength. (B) Wash-out resistance. Mean ± SD; significant difference compared with the control group, *p < 0.05, **p < 0.01.

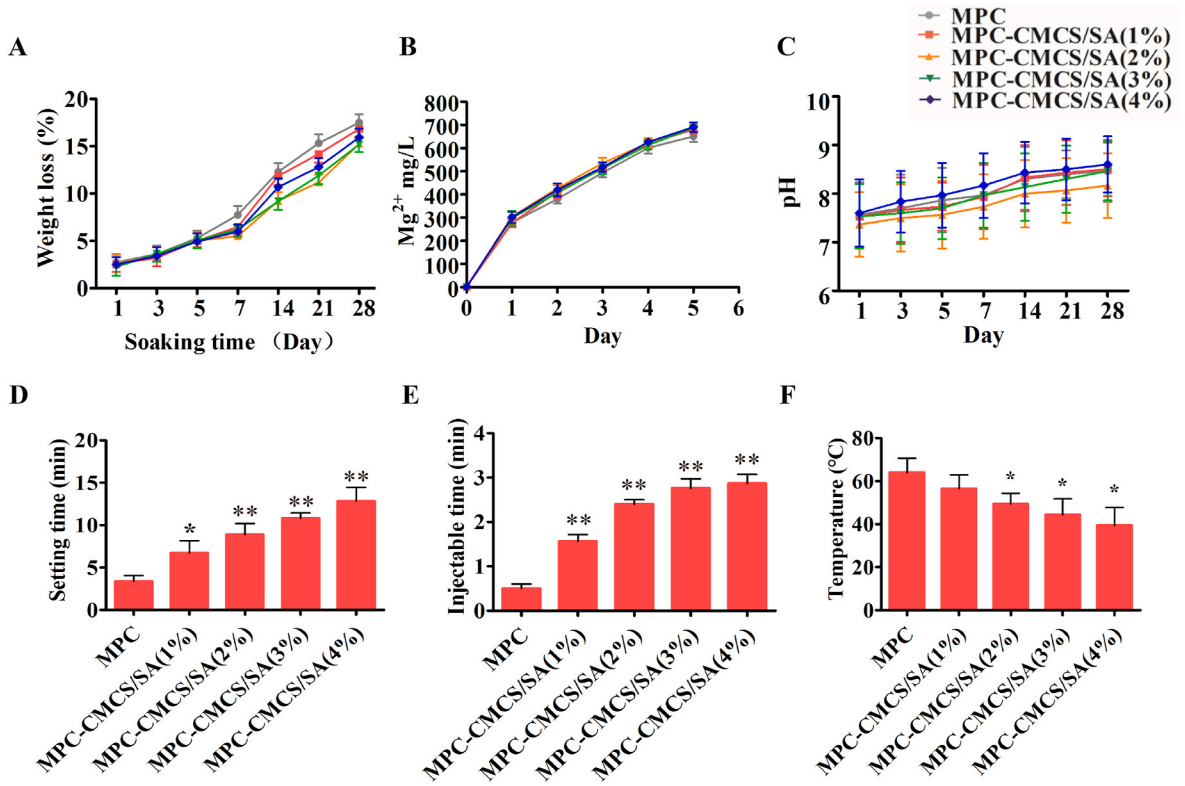

Fig. 2. (A) Weight loss. (B) Mg^{2+} released into medium. (C) pH of immersion medium. (D) Setting time. (E) Injectable time. (F) Temperature. Mean ± SD; significant difference compared with the control group, *p < 0.05, **p < 0.01.

imaging and SEM (Fig. 5). After 24 h of culture on the composites, cells adhered to the surfaces of all samples, indicating favorable biocompatibility for all cement groups. With the increase of CMCS/SA, MC3T3-E1 cells formed more pseudopodia and were distributed more widely. Fiber-like structures were seen on the composite surface, especially when CMCS/SA was added.

Viability of MC3T3-E1 cells in each group was similar on the day 1. However, cells growing on MPC-CMCS/SA exhibited greater proliferation compared with the MPC group on days 3and 5. The OD of MPC-CMCS/SA (1–4%) showed a 1.19 ± 0.17, 1.78 ± 0.28, 1.85 ± 0.20, 1.95 ± 0.21 fold increase compared with MPC on day 3 and a 1.49 ± 0.33, 2.25 ± 0.48, 2.33 ± 0.51, 2.39 ± 0.54 fold increase on day 5 (Fig. 6A). These results indicated that the MPC-CMCS/SA scaffolds had no apparent cytotoxicity.

3.2.2. *Osteogenic differentiation on samples*

We investigated the effect of various scaffolds on osteogenic differentiation of MC3T3-E1 cells by evaluating the expression of three key marker genes (*RUNX2*, *BMP2*, and *OCN*). After the cells were cultured on the composites for 7 and 14 days, expression of osteogenic markers was analyzed by quantitative PCR (Fig. 6B-D) and western blotting (Fig. 6E). We found that MPC-CMCS/SA scaffolds promoted expression of osteogenic proteins compared with the MPC group, and the osteogenic effect was more obvious with the increase of CMCS/SA. In addition, MPC-CMCS/SA scaffolds promoted ALP activity compared to the MPC group (Suppl Fig.1E). These results suggested that CMCS/SA in the

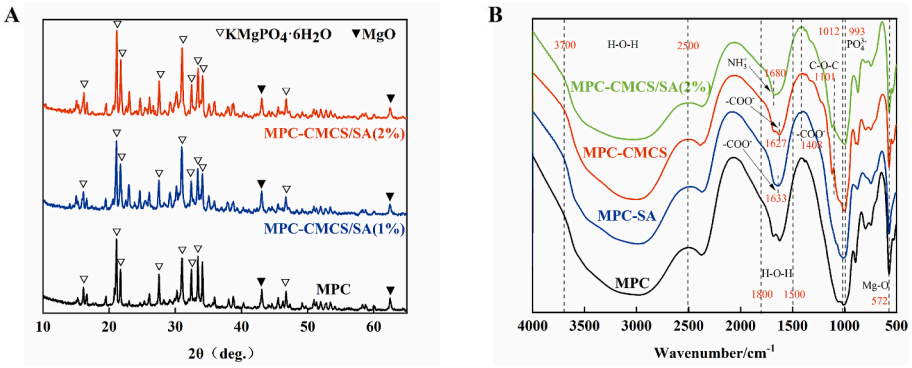

Fig. 3. XRD patterns (A) and FT-IR (B) of different composites.

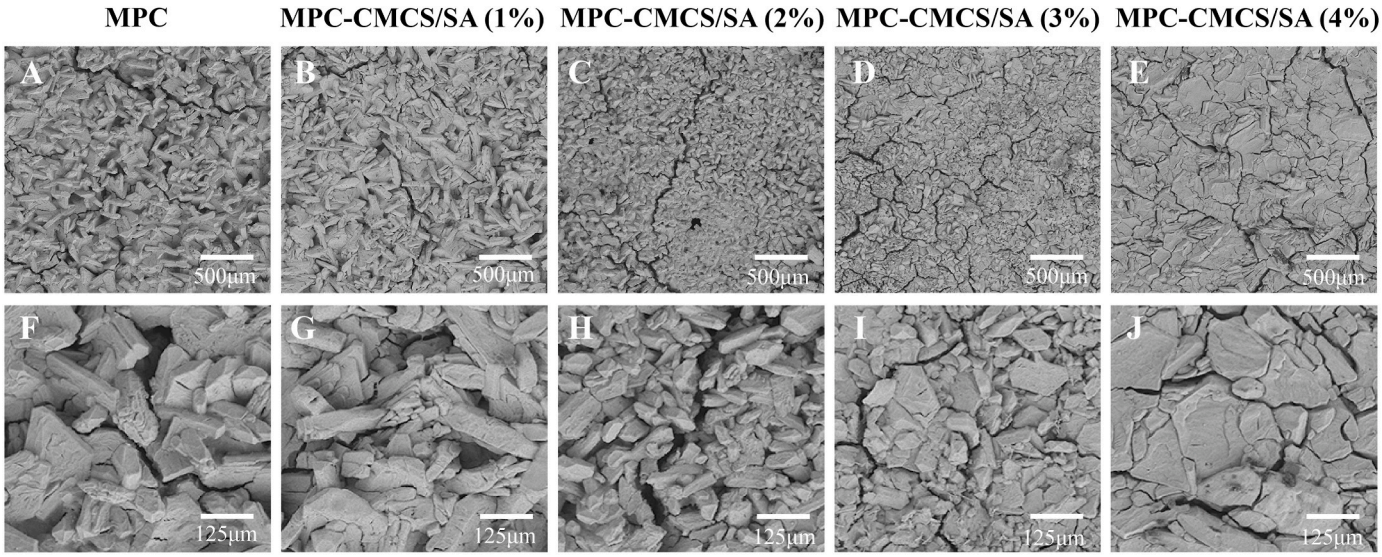

Fig. 4. SEM of the surface morphology of different cements.

scaffolds showed a more pronounced osteogenic differentiation effect on osteoblasts.

3.2.3. Molecular mechanism of enhanced osteogenic differentiation

MPC-CMCS/SA activated the integrin pathway, leading to increased intracellular FAK phosphorylation (Fig. 6F). Cells seeded on MPC-CMCS/SA showed less β-catenin phosphorylation compared with MPC alone. However, when FAK inhibitor (PF-573228; 10 μM; Selleck) was applied to cells cultured on MPC-CMCS/SA, the phosphorylation of β-catenin was significantly increased. In addition, osteogenic genes OCN and RUNX2 were also downregulated after treated by FAK inhibitor (**Suppl Fig.1F**).

3.3. In vivo evaluation of MPC-CMCS/SA scaffolds

3.3.1. In vivo bone regeneration capacities of MPC-CMCS/SA scaffolds

To further determine the *in vivo* bone repair capacity, we constructed critical-sized calvarial defects in rats. Because MPC-CMCS/SA (2%) exhibited the optimal physiochemical properties, it was selected to fill the defects. MPC was set as a control. 3D reconstruction of micro-CT images of the bone defect after implantation for 1 and 3 months are shown in Fig. 6. One month after implantation, scattered regenerated osseous tissue was observed in both cement groups. Three months after transplantation, new bone formation was observed in the central area and at the margins of both implanted samples. In comparison, we found that MPC-CMCS/SA (2%) samples degraded faster than MPC, with thicker and more continuous new bone formation (Fig. 7A).

One month after transplantation, the structural parameters were similar in both groups. After 3 months, however, the MPC-CMCS/SA (2%) group showed significantly higher BV/TV (58.43 ± 6.21% vs. 38.50 ± 5.80%), Tb. N (1.04 ± 0.18 mm^{-1} vs. 0.84 ± 0.19 mm^{-1}), Tb. Th (0.30 ± 0.07 mm vs. 0.22 ± 0.06 mm) and lower Tb. Sp (0.38 ± 0.11 mm vs. 0.41 ± 0.08 mm) compared to the MPC group (Fig. 7B–E).

3.3.2. Histological analysis of in vivo specimens

After micro-CT analysis, specimens were assessed histologically. Representative images of sections stained with H&E, von Kossa and Masson's trichrome were shown in Fig. 8. The Sham group showed no self-healing of the defects (Suppl Fig.1C-D). There was no sign of inflammation, necrosis or infection at the implantation site, implicating the favorable biocompatibility of the cements.

One month after transplantation, a small amount bone formation was observed at the dural side in both groups. At 3 months after implantation, histologically, there were new bone formation and material degradation in both groups. Moreover, blood vessels emerged in the newly formed bone. In comparison, there was more extensive trabeculae and blood vessel formation in the MPC-CMCS/SA (2%) group than in the MPC group. On the contrary, more fibrous tissue was found in the MPC group. These data revealed that cements incorporating CMCS/SA improved critical bone defect repair compared with MPC alone.

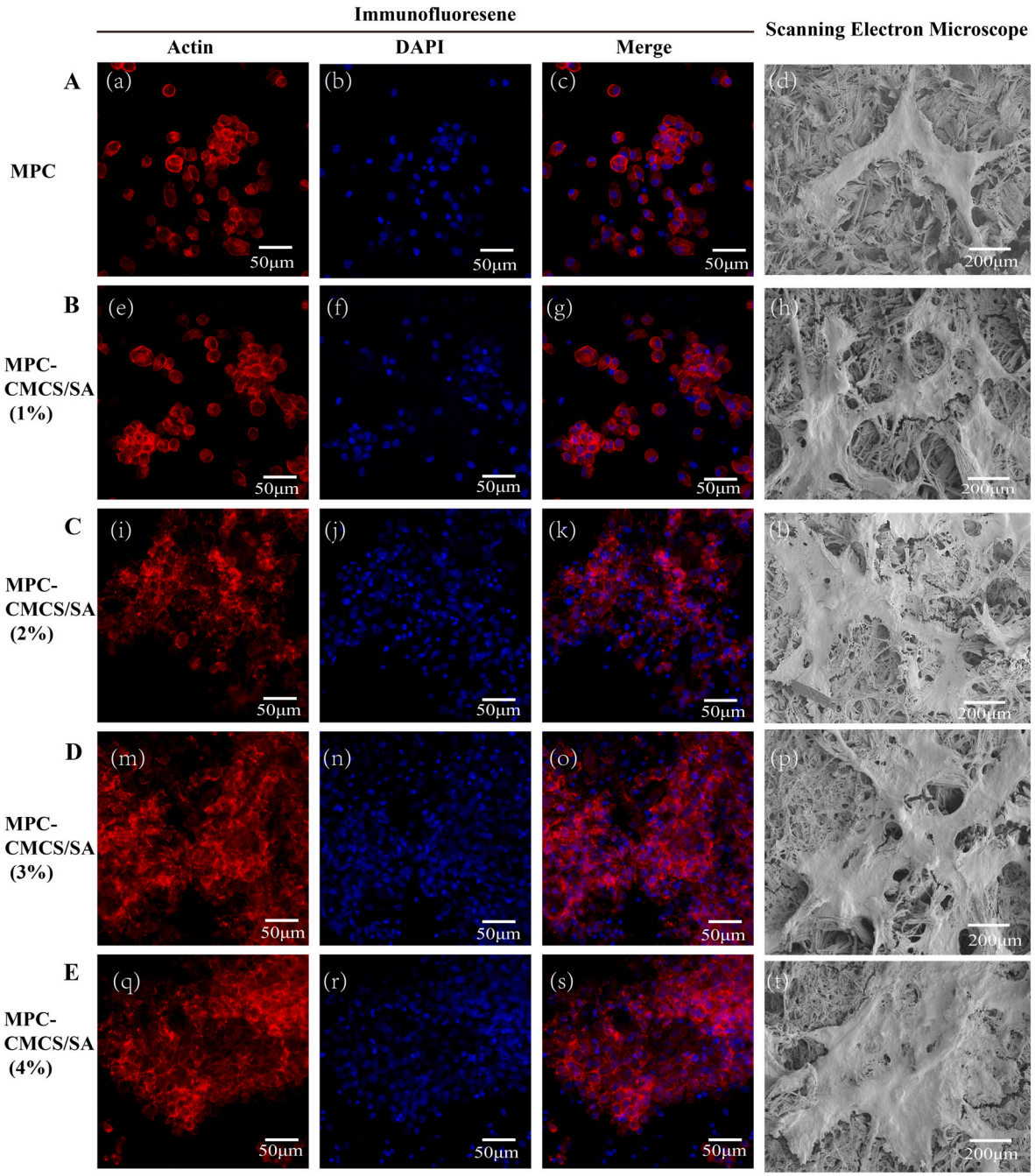

Fig. 5. Immunofluorescence and SEM observation of cell adhesion on (A) MPC, (B) MPC-CMCS/SA (1%), (C) MPC-CMCS/SA (2%), (D) MPC-CMCS/SA (3%) and (E) MPC-CMCS/SA (4%).

4. Discussion

A previous study showed that addition of chitosan-alginate complex to the CPC bone cement system resulted in significantly improved functional properties, such as controllable setting reaction, favorable injectability and increased *in vivo* bone repair [34]. Another study added alginate-chitosan gel system as an internal polymeric gel network into TCP bone cement, which allowed for better clinical handling and mechanical properties of the cement [35]. The current work built on our previous study on optimized MPC cements for bone defect repair [30,36,37]. Here we prepared a novel organic-inorganic bone cement by incorporating CMCS and SA into MPC.

According to the literature, the compressive strength of human cortical bone is 90–190 MPa [38]. As bone substitutes, the mechanical properties of MPC need to be improved. Previously, our group incorporated CMCS into MPC, and increased the compressive strength to ~50 MPa [30]. Consistent with our previous study, the compressive strength first increased and then decreased with the increase of CMCS/SA. However, MPC-CMCS/SA (2%) achieved the highest compressive strength of ~60 MPa, which was about 1.2-times greater than our previous results. This was primarily because SA forms strong electrostatic interaction with CMCS, and can be ionically cross-linked by divalent Mg^{2+} cations. As higher (>4%) CMCS/SA incorporation impaired the compressive strength and wash-out resistance, 1–4%wt of CMCS/SA was utilized for subsequent experiments. In addition, within this concentration range, the CMCS/SA applied had no effect on the *in vitro* degradation, release of Mg^{2+} and pH value.

The reaction of MPC begins with the dissolution of the oxide into

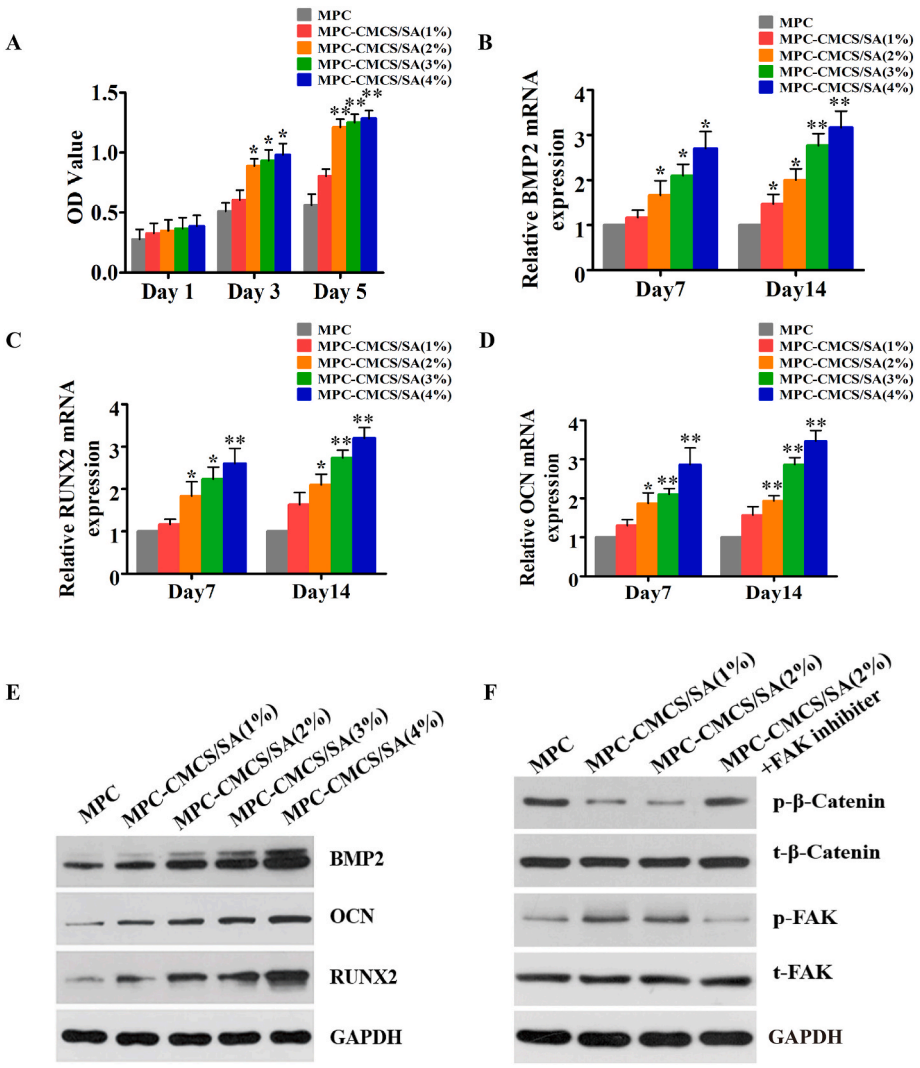

Fig. 6. (A) Cell proliferation on the scaffolds. (B–E) Osteogenic differentiation on the scaffolds. The osteogenic gene markers *BMP2*, *Runx2* and *OCN* were determined using quantitative PCR and western-blotting. (F) FAK-Wnt signaling pathways related genes expression of MC3T3-E1 cells cultured on different cements with/without FAK inhibitor Mean ± SD; significant difference compared with the control group, *$p < 0.05$, **$p < 0.01$.

solution, and the dissolved Mg^{2+} cations react with the phosphate anions. Therefore, the solidification rate mainly depends on the dissolution process [16]. The hydrogel in the composite prolonged the dissolution step, and extended the setting process. The injectable time of MPC-CMCS/SA composite also significantly extended with the increase of CMCS/SA. During the setting process, the exothermic hydration reaction produces sharp exothermic peaks, which could damage surrounding tissue *in vivo*. Indeed, the maximum temperature of MPC reached ~64 °C. We observed that adding CMCS and SA decreased the maximum temperature to ~39 °C, which was primarily due to the extended setting reaction. The improved injectability and extended setting time are beneficial for clinical applications.

There were no secondary hydration products according to XRD analysis, which suggested that CMCS and SA were not involved in the hydration products. In accordance with a previous study, the spectra of MPC products showed the characteristic peaks of PO_4^{3-} and Mg–O [39]. The spectrum of MPC-SA and MPC-CMCS/SA showed a normal symmetric stretching peak but a shift of COO^- asymmetric stretching peak to a higher wave number from 1595 to 1633 cm^{-1}, which was attributed to a strong interaction between the carboxylic group and the Mg^{2+} ions [40]. In addition, the spectrum of MPC-CMCS/SA showed a shift in the variable angle vibration of NH_2 to the asymmetric variable angle vibration of NH_3^+ at 1680 cm^{-1}, which indicated the electrostatic interaction between CMCS and SA [27]. The surface morphology of bone cement was important with respect to cellular adhesion and proliferation. During setting, CMCS/SA acted as micro-filler, and addition of CMCS/SA caused the crystals to become finer and made the surface of the composites smoother.

Cell adhesion occurs in the early stage of tissue regeneration, and effective cell adhesion provides the basis for subsequent biological functions, including cell proliferation and differentiation [41]. MC3T3-E1 cells on MPC-CMCS/SA formed more pseudopodia and spread more widely. This was probably due to the ECM-like structure in CMCS, which provides more binding sites for the initial cell attachment [25]. In addition, intersected bundles of fibers can be clearly seen on the surface after co-culture with osteoblast cells, which indicated the formation of an extracellular microenvironment favorable for cell recruitment. According to our previous study [30], we speculated that CMCS/SA would promote fibronectin adsorption and subsequent integrin signaling activation. These results indicated that the MPC-CMCS/SA scaffolds showed excellent cytocompatibility.

Tight control of different molecular factors exerts an important influence on differentiation to the osteogenic lineage [42]. The most important positive regulator of osteoblast differentiation is BMP2, which has been shown to activate the Smad signaling cascade and Runx2. Runx2 specifically regulates the expressions of osteogenic genes during

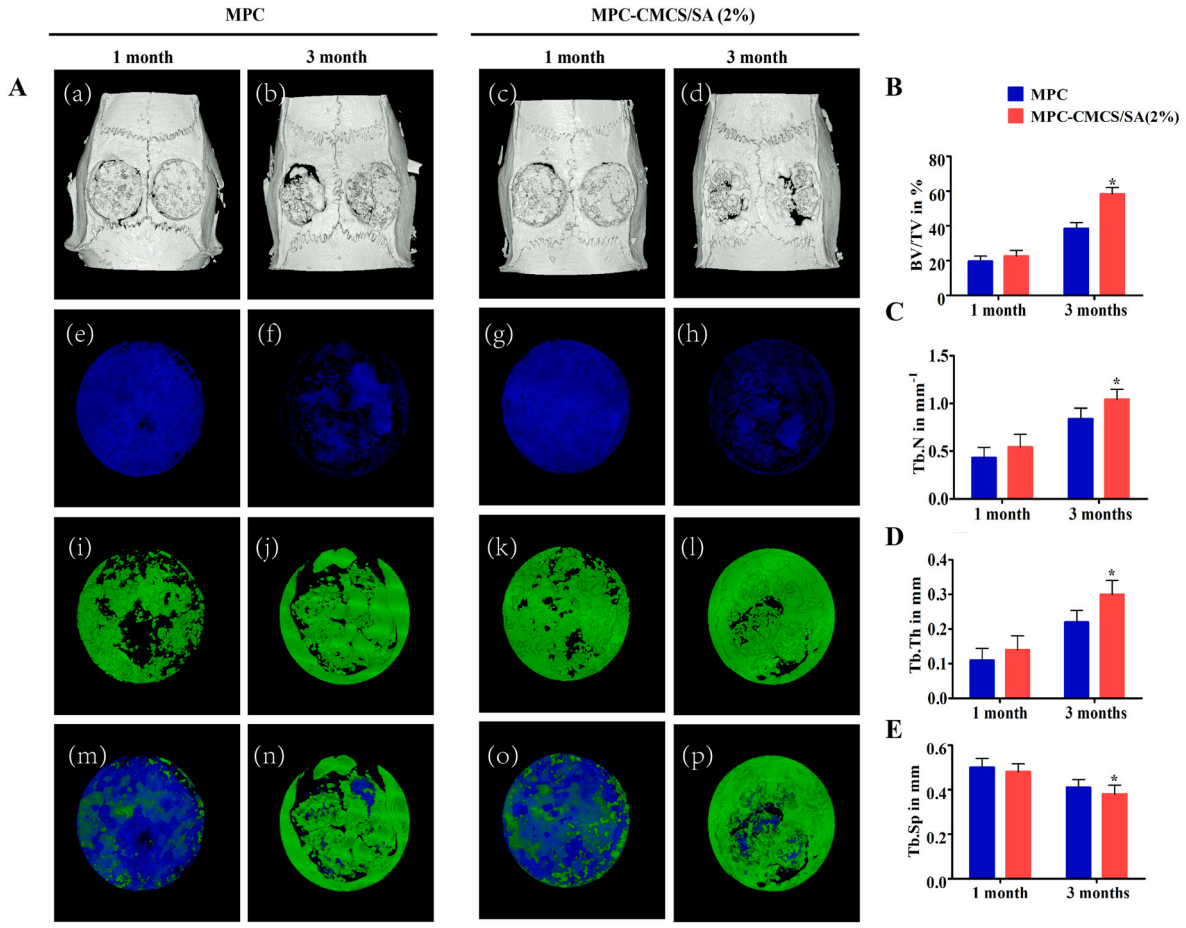

Fig. 7. (A) 3D reconstructed images of the area with implantation of MPC and MPC-CMCS/SA (2%) in rat calvaria defects at 1 and 3 months (blue area presenting implanted scaffolds and green area indicating new bone formation). (B–E) Bone structural parameters of the rat calvaria defects with different cements implantation at 1 and 3 months. Mean ± SD; significant difference compared with the control group, *$p < 0.05$, **$p < 0.01$.

osteoblast differentiation, including osteocalcin; a late marker for osteogenic differentiation. Our data suggested that CMCS/SA in the scaffolds induced a more pronounced osteogenic differentiation effect on osteoblasts.

An indispensable factor in adhesion-dependent signaling and osteogenesis is focal adhesion kinase (FAK) [43]. Previously, we found that CMPC adsorbed more fibronectin, bound integrin receptors, activated the integrin-FAK pathway, and induced the osteogenic differentiation of MC3T3-E1 cells [30]. Wnt signaling is inextricably linked with the regulation of bone mass. Since β-catenin is the core molecule of the canonical Wnt pathway, it plays a crucial role in osteogenesis [44]. Upon Wnt activation, β-catenin first translocates into the nuclei and then binds to the T-cell factor/lymphoid enhancer factor family of transcription factors, thereby promoting the transcription of target genes such as Jun and c-Myc. In the absence of Wnt ligands, β-catenin is recruited to the destruction complex that contains adenomatous polyposis coli (APC) and axis inhibition protein (AXIN), which facilitates the phosphorylation of β-catenin and subsequent ubiquitination and proteasomal degradation [45]. It is been reported that FAK regulated disordered protein (Dvl) and then disrupted the APC/Axin/GSK-3β complex, thereby reducing the phosphorylation of β-catenin [46]. We examined whether FAK regulateed β-catenin phosphorylation. A FAK inhibitor (PF-573228; 10 μM) was applied to cells cultured on MPC-CMCS/SA, and its efficacy was confirmed by decreased FAK phosphorylation. As expected, β-catenin showed increased phosphorylation upon FAK inhibition. This implies that FAK, as a downstream effector of itegrin, could regulate phosphorylation of β-catenin, and then regulate osteogenic differentiation. Furthermore, the osteogenic genes were also downregulated after treated by FAK inhibitor, further confirming that FAK is a key regulator on osteogenesis. We thus suggest a novel integrin-FAK-Wnt axis in MPC-CMCS/SA enhanced osteogenic differentiation.

Based on the physicochemical properties and the *in vitro* response to the cements, MPC-CMCS/SA (2%) were selected to evaluate the capacity to heal critical-size defects in a rat calvaria defect model *in vivo*, and MPC was set as control. The Sham group showed no self-healing, confirming the defects were of critical-size. In our study, we observed that bone formation started from the dura mater side in both of the two cements, which meant that the dura mater may transport precursor cells into the bone defect in the early phase. The osteogenic effects of CMCS/SA were reported in various studies. Lu et al. [47] constructed a scaffold of copper-containing CMCS/SA that could be used to simultaneously eradicate bacterial infection and promote bone formation. Tao et al. [48] fabricated a polycaprolactone/CMCS/SA fibers, and found that the microfibers played a positive role in osteoblast viability and osteogenesis. Consistently, the enhanced *in vivo* osteogenic capacity for MPC-CMCS/SA in our study was confirmed by more new bone and vascular formation around the implants. In the future, our composites could be further improved by incorporating modern strategies such as bone regenerative exosomes [49,50].

5. Conclusions

We successfully developed a novel bone cement composite by adding CMCS and SA to magnesium phosphate bone cement. CMCS/SA improved the mechanical strength and decreased heat release of MPC

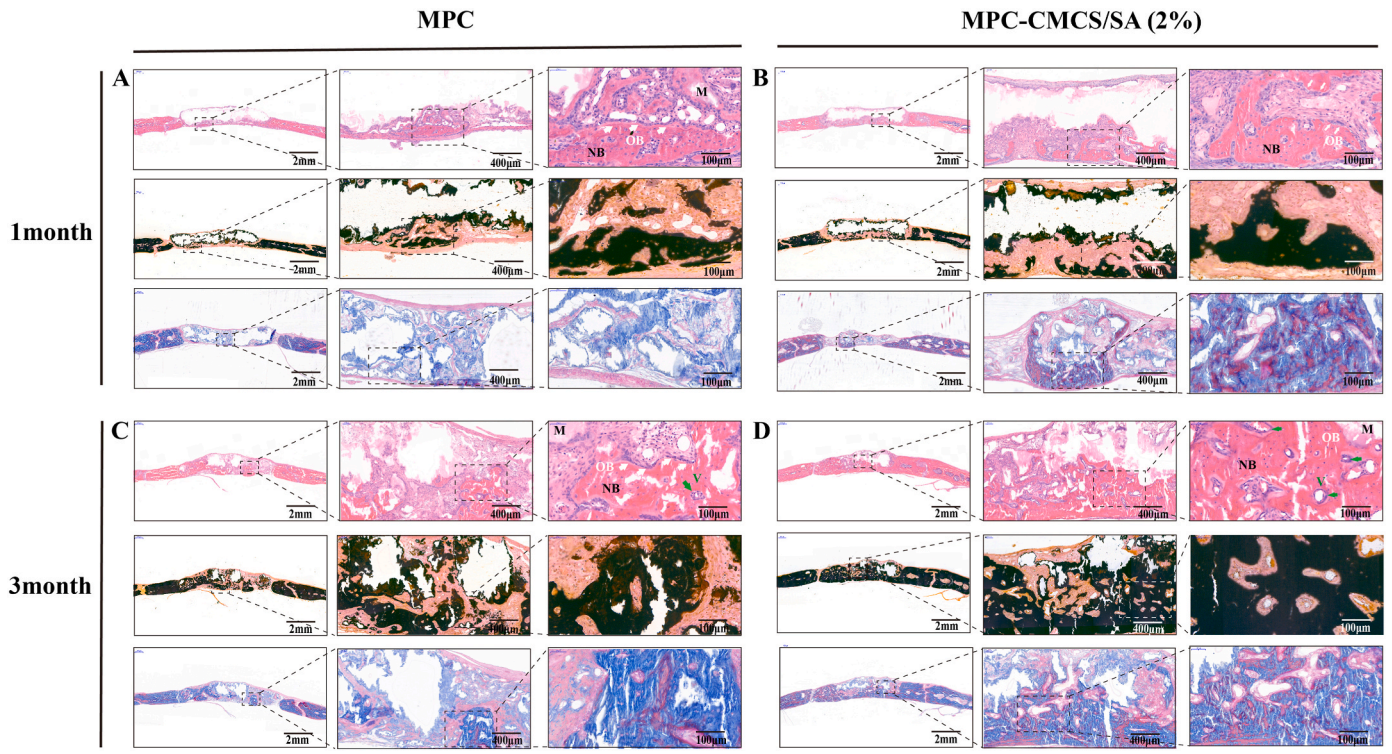

Fig. 8. H&E, von Kossa and Masson staining of the MPC and MPC-CMCS/SA scaffolds *in vivo*. (A) 1month and (B) 3month after MPC transplantation. (C) 1month and (D)3month after MPC-CMCS/SA (2%) transplantation. (M: materials, NB: new bone formation, OB and white arrows: osteoblasts, V and green arrows: new vascular formation).

cement that would favor *in vivo* strength while minimizing tissue damage. The MPC-CMCS/SA composite had a longer setting time and gel-like handling characteristic, making it easily manipulable for clinical application. *In vitro* studies suggested that MPC-CMCS/SA had good biocompatibility, and facilitated cell adhesion and proliferation. Furthermore, the MPC-CMCS/SA composite enhanced osteogenic differentiation *in vitro* through the integrin-FAK-Wnt axis. *In vivo* studies of rat calvaria defect demonstrated that the MPC-CMCS/SA composite enhanced critical bone defect repair. Therefore, MPC-CMCS/SA showed remarkable potential for bone tissue repair and regeneration.

Funding statement

The present study was completed with the support of the National Natural Science Foundation of China (No. 81802689 and 51772233), the Provincial Key Research and Development Program of Hubei, China (No. 2020BCB058), State Key Laboratory of Advanced Technology for Materials Synthesis and Processing (Wuhan University of Technology) (2021-KF-22), the Major Special Projects of Technological Innovation of Hubei Province (No.2019ACA130), and the Application Foundation and Front Research Program of Wuhan (No. 2018010401011273).

Ethics approval and consent to participate

All *in vivo* experiments were reviewed and approved by the Investigational Ethical Review Board of Renmin Hospital of Wuhan University. The ethical committee had confirmed authors' compliance with all relevant ethical regulations.

CRediT authorship contribution statement

Ling Yu: Formal analysis, Data curation, Writing – original draft. **Tian Gao:** Validation, Investigation. **Wei Li:** Formal analysis, Data curation, Writing – original draft. **Jian Yang:** Resources. **Yinchu Liu:** Investigation. **Yanan Zhao:** Validation. **Ping He:** Investigation. **Xuefeng Li:** Validation. **Weichun Guo:** Writing – review & editing, Supervision, Project administration. **Zhengfu Fan:** Writing – review & editing, Supervision. **Honglian Dai:** Writing – review & editing, Supervision.

Declaration of competing interest

The authors declare that they have no known competing financial interests or personal relationships that could have appeared to influence the work reported in this paper.

Abbreviations

MPC	magnesium phosphate cement
CMCS	carboxymethyl chitosan
SA	Sodium alginate
BMP2	bone morphogenetic protein 2
OCN	osteocalcin
RUNX2	runt-related transcription factor 2

Appendix A. Supplementary data

Supplementary data to this article can be found online at https://doi.org/10.1016/j.bioactmat.2022.06.017.

References

[1] B. Wildemann, A. Ignatius, F. Leung, L.A. Taitsman, R.M. Smith, R. Pesantez, M. J. Stoddart, R.G. Richards, J.B. Jupiter, Non-union bone fractures, Nat. Rev. Dis. Prim. 7 (1) (2021) 57, https://doi.org/10.1038/s41572-021-00289-8.
[2] G.S. Marecek, M.T. Little, M.J. Gardner, M. Stevanovic, R. Lefebvre, M. Bernstein, Management of critical bone defects, Instr. Course Lect. 69 (2020) 417–432.
[3] T. Winkler, F.A. Sass, G.N. Duda, K. Schmidt-Bleek, A review of biomaterials in bone defect healing, remaining shortcomings and future opportunities for bone

tissue engineering: the unsolved challenge, Bone Joint Res. 7 (3) (2018) 232–243, https://doi.org/10.1302/2046-3758.73.BJR-2017-0270.R1.
[4] W. Wang, K.W.K. Yeung, Bone grafts and biomaterials substitutes for bone defect repair: a review, Bioact. Mater. 2 (4) (2017) 224–247, https://doi.org/10.1016/j.bioactmat.2017.05.007.
[5] M.D.G.L. Koons, A.G. Mikos, Materials design for bone-tissue engineering, Nat. Rev. Mater. 5 (2020) 584–603, https://doi.org/10.1038/s41578-020-0204-2.
[6] B. Tan, Q. Tang, Y. Zhong, Y. Wei, L. He, Y. Wu, J. Wu, J. Liao, Biomaterial-based strategies for maxillofacial tumour therapy and bone defect regeneration, Int. J. Oral Sci. 13 (1) (2021) 9, https://doi.org/10.1038/s41368-021-00113-9.
[7] W. Zhi, X. Wang, D. Sun, T. Chen, B. Yuan, X. Li, X. Chen, J. Wang, Z. Xie, X. Zhu, K. Zhang, X. Zhang, Optimal regenerative repair of large segmental bone defect in a goat model with osteoinductive calcium phosphate bioceramic implants, Bioact. Mater. 11 (2022) 240–253, https://doi.org/10.1016/j.bioactmat.2021.09.024.
[8] A. Malhotra, P. Habibovic, Calcium phosphates and angiogenesis: implications and advances for bone regeneration, Trends Biotechnol. 34 (12) (2016) 983–992, https://doi.org/10.1016/j.tibtech.2016.07.005.
[9] X. Cui, C. Huang, Z. Chen, M. Zhang, C. Liu, K. Su, J. Wang, L. Li, R. Wang, B. Li, D. Chen, C. Ruan, D. Wang, W.W. Lu, H. Pan, Hyaluronic acid facilitates bone repair effects of calcium phosphate cement by accelerating osteogenic expression, Bioact. Mater. 6 (11) (2021) 3801–3811, https://doi.org/10.1016/j.bioactmat.2021.03.028.
[10] L. Ding, H. Wang, W. Zhang, J. Li, D. Liu, F. Han, S. Chen, B. Li, Calcium phosphate bone cement with enhanced physicochemical properties via in situ formation of an interpenetrating network, J. Mater. Chem. B 9 (34) (2021) 6802–6810, https://doi.org/10.1039/d1tb00867f.
[11] M. Rondanelli, M.A. Faliva, A. Tartara, C. Gasparri, S. Perna, V. Infantino, A. Riva, G. Petrangolini, G. Peroni, An update on magnesium and bone health, Biometals 34 (4) (2021) 715–736, https://doi.org/10.1007/s10534-021-00305-0.
[12] B. He, L. Xia, J. Zhao, L. Yin, M. Zhang, Z. Quan, Y. Ou, W. Huang, Causal effect of serum magnesium on osteoporosis and cardiometabolic diseases, Front. Nutr. 8 (2021), 738000, https://doi.org/10.3389/fnut.2021.738000.
[13] D. Li, D. Zhang, Q. Yuan, L. Liu, H. Li, L. Xiong, X. Guo, Y. Yan, K. Yu, Y. Dai, T. Xiao, Y. Li, C. Wen, In vitro and in vivo assessment of the effect of biodegradable magnesium alloys on osteogenesis, Acta Biomater. 141 (2022) 454–465, https://doi.org/10.1016/j.actbio.2021.12.032.
[14] Y. Zhang, J. Xu, Y.C. Ruan, M.K. Yu, M. O'Laughlin, H. Wise, D. Chen, L. Tian, D. Shi, J. Wang, S. Chen, J.Q. Feng, D.H. Chow, X. Xie, L. Zheng, L. Huang, S. Huang, K. Leung, N. Lu, L. Zhao, H. Li, D. Zhao, X. Guo, K. Chan, F. Witte, H. C. Chan, Y. Zheng, L. Qin, Implant-derived magnesium induces local neuronal production of CGRP to improve bone-fracture healing in rats, Nat. Med. 22 (10) (2016) 1160–1169, https://doi.org/10.1038/nm.4162.
[15] W. Qiao, K.H.M. Wong, J. Shen, W. Wang, J. Wu, J. Li, Z. Lin, Z. Chen, J. P. Matinlinna, Y. Zheng, S. Wu, X. Liu, K.P. Lai, Z. Chen, Y.W. Lam, K.M.C. Cheung, K.W.K. Yeung, TRPM7 kinase-mediated immunomodulation in macrophage plays a central role in magnesium ion-induced bone regeneration, Nat. Commun. 12 (1) (2021) 2885, https://doi.org/10.1038/s41467-021-23005-2.
[16] N. Ostrowski, A. Roy, P.N. Kumta, Magnesium phosphate cement systems for hard tissue applications: a review, ACS Biomater. Sci. Eng. 2 (7) (2016) 1067–1083, https://doi.org/10.1021/acsbiomaterials.6b00056.
[17] B. Kanter, A. Vikman, T. Bruckner, M. Schamel, U. Gbureck, A. Ignatius, Bone regeneration capacity of magnesium phosphate cements in a large animal model, Acta Biomater. 69 (2018) 352–361, https://doi.org/10.1016/j.actbio.2018.01.035.
[18] S. Yu, L. Liu, C. Xu, H. Dai, Magnesium phosphate based cement with improved setting, strength and cytocompatibility properties by adding Ca(H2PO4)2.H2O and citric acid, J. Mech. Behav. Biomed. Mater. 91 (2019) 229–236, https://doi.org/10.1016/j.jmbbm.2018.12.004.
[19] S. Wang, C. Xu, S. Yu, X. Wu, Z. Jie, H. Dai, Citric acid enhances the physical properties, cytocompatibility and osteogenesis of magnesium calcium phosphate cement, J. Mech. Behav. Biomed. Mater. 94 (2019) 42–50, https://doi.org/10.1016/j.jmbbm.2019.02.026.
[20] D. Lopes, C. Martins-Cruz, M.B. Oliveira, J.F. Mano, Bone physiology as inspiration for tissue regenerative therapies, Biomaterials 185 (2018) 240–275, https://doi.org/10.1016/j.biomaterials.2018.09.028.
[21] R. Sergi, D. Bellucci, V. Cannillo, A review of bioactive glass/natural polymer composites: state of the art, Materials 13 (23) (2020), https://doi.org/10.3390/ma13235560.
[22] L.G. Confederat, C.G. Tuchilus, M. Dragan, M. Sha'at, O.M. Dragostin, Preparation and antimicrobial activity of chitosan and its derivatives: a concise review, Molecules 26 (12) (2021), https://doi.org/10.3390/molecules26123694.
[23] S. Sharma, P. Sudhakara, J. Singh, R.A. Ilyas, M.R.M. Asyraf, M.R. Razman, Critical review of biodegradable and bioactive polymer composites for bone tissue engineering and drug delivery applications, Polymers 13 (16) (2021), https://doi.org/10.3390/polym13162623.
[24] Z. Jiang, L. Li, H. Li, L. Xia, H. Hu, S. Wang, C. Liu, J. Chi, Y. Yang, F. Song, W. Liu, B. Han, Preparation, biocompatibility, and wound healing effects of O-carboxymethyl chitosan nonwoven fabrics in partial-thickness burn model, Carbohydr. Polym. 280 (2022), 119032, https://doi.org/10.1016/j.carbpol.2021.119032.
[25] Z. Shariatinia, Carboxymethyl chitosan: properties and biomedical applications, Int. J. Biol. Macromol. 120 (Pt B) (2018) 1406–1419, https://doi.org/10.1016/j.ijbiomac.2018.09.131.
[26] K.Y. Lee, D.J. Mooney, Alginate: properties and biomedical applications, Prog. Polym. Sci. 37 (1) (2012) 106–126, https://doi.org/10.1016/j.progpolymsci.2011.06.003.
[27] L. Wang, L. Sun, Z. Gu, W. Li, L. Guo, S. Ma, L. Guo, W. Zhang, B. Han, J. Chang, N-carboxymethyl chitosan/sodium alginate composite hydrogel loading plasmid DNA as a promising gene activated matrix for in-situ burn wound treatment, Bioact. Mater. 15 (2022) 330–342, https://doi.org/10.1016/j.bioactmat.2021.12.012.
[28] X. Wu, H. Li, Incorporation of bioglass improved the mechanical stability and bioactivity of alginate/carboxymethyl chitosan hydrogel wound dressing, ACS Appl. Bio Mater. 4 (2) (2021) 1677–1692, https://doi.org/10.1021/acsabm.0c01477.
[29] H. Jing, X. Huang, X. Du, L. Mo, C. Ma, H. Wang, Facile synthesis of pH-responsive sodium alginate/carboxymethyl chitosan hydrogel beads promoted by hydrogen bond, Carbohydr. Polym. 278 (2022), 118993, https://doi.org/10.1016/j.carbpol.2021.118993.
[30] L. Yu, K. Xia, C. Gong, J. Chen, W. Li, Y. Zhao, W. Guo, H. Dai, An injectable bioactive magnesium phosphate cement incorporating carboxymethyl chitosan for bone regeneration, Int. J. Biol. Macromol. 160 (2020) 101–111, https://doi.org/10.1016/j.ijbiomac.2020.05.161.
[31] J. Han, Z. Zhou, R. Yin, D. Yang, J. Nie, Alginate-chitosan/hydroxyapatite polyelectrolyte complex porous scaffolds: preparation and characterization, Int. J. Biol. Macromol. 46 (2) (2010) 199–205, https://doi.org/10.1016/j.ijbiomac.2009.11.004.
[32] Z. Zou, L. Wang, Z. Zhou, Q. Sun, D. Liu, Y. Chen, H. Hu, Y. Cai, S. Lin, Z. Yu, B. Tan, W. Guo, Z. Ling, X. Zou, Simultaneous incorporation of PTH(1-34) and nano-hydroxyapatite into Chitosan/Alginate Hydrogels for efficient bone regeneration, Bioact. Mater. 6 (6) (2021) 1839–1851, https://doi.org/10.1016/j.bioactmat.2020.11.021.
[33] D. Shi, J. Shen, Z. Zhang, C. Shi, M. Chen, Y. Gu, Y. Liu, Preparation and properties of dopamine-modified alginate/chitosan-hydroxyapatite scaffolds with gradient structure for bone tissue engineering, J. Biomed. Mater. Res. 107 (8) (2019) 1615–1627, https://doi.org/10.1002/jbm.a.36678.
[34] H.J. Lee, B. Kim, A.R. Padalhin, B.T. Lee, Incorporation of chitosan-alginate complex into injectable calcium phosphate cement system as a bone graft material, Mater. Sci. Eng. C Mater. Biol .Appl. 94 (2019) 385–392, https://doi.org/10.1016/j.msec.2018.09.039.
[35] J.Z.Y. Huang, W. Zhang, S. Zeng, H. Shi, T. Yu, C. Zhou, Formulation of α-tricalcium phosphate bone cement based on an alginate-chitosan gel system, Cryst. Growth Des. 20 (3) (2020) 1400–1404, https://doi.org/10.1021/acs.cgd.0c00005.
[36] C. Gong, S. Fang, K. Xia, J. Chen, L. Guo, W. Guo, Enhancing the mechanical properties and cytocompatibility of magnesium potassium phosphate cement by incorporating oxygen-carboxymethyl chitosan, Regen. Biomater. 8 (1) (2021), https://doi.org/10.1093/rb/rbaa048 rbaa048.
[37] Y. Shi, L. Yu, C. Gong, W. Li, Y. Zhao, W. Guo, A bioactive magnesium phosphate cement incorporating chondroitin sulfate for bone regeneration, Biomed. Mater. 16 (3) (2021), https://doi.org/10.1088/1748-605X/abf5c4.
[38] E.F. Morgan, G.U. Unnikrisnan, A.I. Hussein, Bone mechanical properties in healthy and diseased states, Annu. Rev. Biomed. Eng. 20 (2018) 119–143, https://doi.org/10.1146/annurev-bioeng-062117-121139.
[39] M.A.H.X. Man, B. Chen, Engineering properties and microstructure analysis of magnesium phosphate cement mortar containing bentonite clay, Construct. Build. Mater. 227 (2019), https://doi.org/10.1016/j.jclepro.2022.130882.
[40] J. Li, J. He, Y. Huang, D. Li, X. Chen, Improving surface and mechanical properties of alginate films by using ethanol as a co-solvent during external gelation, Carbohydr. Polym. 123 (2015) 208–216, https://doi.org/10.1016/j.carbpol.2015.01.040.
[41] C.F. Guimaraes, A.P. Marques, R.L. Reis, Pushing the natural frontier: progress on the integration of biomaterial cues towards combinatorial biofabrication and tissue engineering, Adv. Mater. (2022), e2105645, https://doi.org/10.1002/adma.202105645.
[42] M. Ponzetti, N. Rucci, Osteoblast differentiation and signaling: established concepts and emerging topics, Int. J. Mol. Sci. 22 (13) (2021), https://doi.org/10.3390/ijms22136651.
[43] X. Sun, W. Zheng, C. Qian, Q. Wu, Y. Hao, G. Lu, Focal adhesion kinase promotes BMP2-induced osteogenic differentiation of human urinary stem cells via AMPK and Wnt signaling pathways, J. Cell. Physiol. 235 (5) (2020) 4954–4964, https://doi.org/10.1002/jcp.29374.
[44] R. Baron, M. Kneissel, WNT signaling in bone homeostasis and disease: from human mutations to treatments, Nat. Med. 19 (2) (2013) 179–192, https://doi.org/10.1038/nm.3074.
[45] J. Liu, Q. Xiao, J. Xiao, C. Niu, Y. Li, X. Zhang, Z. Zhou, G. Shu, G. Yin, Wnt/beta-catenin signalling: function, biological mechanisms, and therapeutic opportunities, Signal Transduct. Targeted Ther. 7 (1) (2022) 3, https://doi.org/10.1038/s41392-021-00762-6.
[46] S.P. Crampton, B. Wu, E.J. Park, J.H. Kim, C. Solomon, M.L. Waterman, C. C. Hughes, Integration of the beta-catenin-dependent Wnt pathway with integrin signaling through the adaptor molecule Grb2, PLoS One 4 (11) (2009), e7841, https://doi.org/10.1371/journal.pone.0007841.
[47] Y. Lu, L. Li, Y. Zhu, X. Wang, M. Li, Z. Lin, X. Hu, Y. Zhang, Q. Yin, H. Xia, C. Mao, Multifunctional copper-containing carboxymethyl chitosan/alginate scaffolds for eradicating clinical bacterial infection and promoting bone formation, ACS Appl. Mater. Interfaces 10 (1) (2018) 127–138, https://doi.org/10.1021/acsami.7b13750.
[48] Y.C.F. Tao, H. Tao, L. Jin, Z. Wan, F. Dai, W. Xiang, H. Deng, Carboxymethyl chitosan/sodium alginate-based micron-fibers fabricated by emulsion

electrospinning for periosteal tissue engineering, Mater. Des. 194 (2020), 108849, https://doi.org/10.1016/j.matdes.2020.108849.
[49] M. Zhai, Y. Zhu, M. Yang, C. Mao, Human mesenchymal stem cell derived exosomes enhance cell-free bone regeneration by altering their miRNAs profiles, Adv. Sci. 7 (19) (2020), 2001334, https://doi.org/10.1002/advs.202001334.
[50] J. Sun, Z. Yin, X. Wang, J. Su, Exosome-laden hydrogels: a novel cell-free strategy for in-situ bone tissue regeneration, Front. Bioeng. Biotechnol. 10 (2022), 866208, https://doi.org/10.3389/fbioe.2022.866208.